

Low-Threshold Nanowire Laser Based on Composition-Symmetric Semiconductor Nanowires

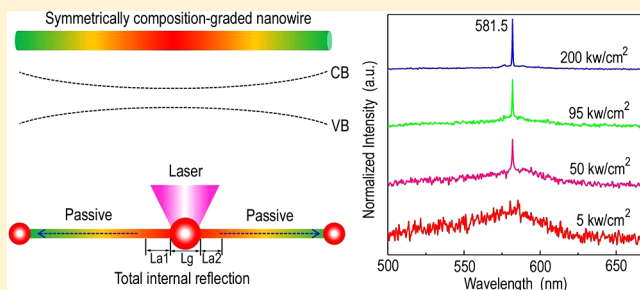
Pengfei Guo, Xiujuan Zhuang, Jinyou Xu, Qinglin Zhang, Wei Hu, Xiaoli Zhu, Xiaoxia Wang, Qiang Wan, Pengbin He, Hong Zhou, and Anlian Pan*

Key Laboratory for Micro-Nano Physics and Technology of Hunan Province, State Key Laboratory of Chemo/Biosensing and Chemometrics, College of Physics and Microelectronics Science, Hunan University, Changsha 410082, China

Supporting Information

ABSTRACT: Low-threshold nanoscale lasers are attractive for their promising applications in highly integrated photonic devices and systems. Here we report the controllable growth of composition-symmetric $\text{CdS}_x\text{Se}_{1-x}$ nanowires by using a multistep thermal evaporation route with moving sources. Microstructure analyses reveal the obtained wires are high-quality single crystals with the composition gradually changed from the center toward their both ends. Under laser illumination, these wires exhibit symmetrical color distribution along the length direction, with red at the center and green at the both ends. Optically pumped lasing is realized at room temperature using these composition-symmetric nanowires, with the threshold several times lower than that of composition-homogeneous wires. This new nanowire structure will have potential applications as low-threshold nanoscale lasers in integrated nanophotonics.

KEYWORDS: Low-threshold, nanowire laser, composition-symmetric, nanophotonics



Rational design and control of the composition of nanostructures are important in yielding enhanced and/or enriched electronic and photonic functions for their high-performance applications in nanoscale electronics and photonics devices.^{1–5} For example, Ge/Si nanowire (NW) heterostructures exhibit substantially excellent performance as field-effect transistors compared with those structures of homogeneous composition.¹ A semiconductor laser of a energy-band engineered quantum well structure can lower the lasing threshold by introducing a substantial density of states at the band edges.²

Low-threshold nanoscale lasers are promising for applications in high-throughput sensing and optical communication.^{2,6–12} One-dimensional (1D) semiconductor NWs can simultaneously function as both active gain material and optical waveguide cavities for their high refractive index contrast to the surroundings^{13–20} and act as ideal nanoscale lasers for highly integrated photonic applications.^{21–26} However, conventional semiconductor NW lasers are subjected to relatively high lasing threshold, owing to their high self-absorption energy loss^{27–29} and/or low end-face reflection.¹³ In regular composition-homogeneous semiconductor NWs (Figure 1A), the bandgap has an unchanged value along their whole length (Figure 1B). When the NW is intermediately excited by a focused laser beam, the excited light will be actively guided toward the two opposite ends through the reabsorption and re-emitting (Figure 1C).³⁰ Consequently, the propagation loss (both optical intensity and photonic energy) of the guiding light is quite

large, leading to a high lasing threshold.^{27–29} So far, there are lack of effective methods on the lowering of nanoscale laser threshold by reducing self-absorption loss.

In this work, we design a low-loss NW cavity by constructing a symmetrical composition distribution along the wire length. As schematically shown in Figure 1D, the composition along this symmetric NW is gradually changed from the center to the two ends, resulting in the center of the wire having a minimum bandgap value (Figure 1E). When the central region of the NW is locally excited by a focused laser beam (Figure 1F), the emitted light will be passively guided toward the two opposite ends with almost no self-absorption, since the photon energy of the emitted light is smaller than the bandgap of any other positions along the two opposite propagating direction. As a result, the propagation loss of the guiding light in these symmetrically composition-graded NWs is expected to be much smaller than the active waveguiding process in common composition-homogeneous NWs,^{30,31} since the self-absorption induced optical loss cannot take place in these symmetric wires. Experimentally, we successfully grew such symmetrically composition-graded NWs through a source-controlled thermal evaporation route. Optical pumping of individual NW structures demonstrates that the lasing threshold is several times lower than that of composition-homogeneous NWs. This

Received: December 29, 2012

Revised: February 8, 2013

Published: February 19, 2013



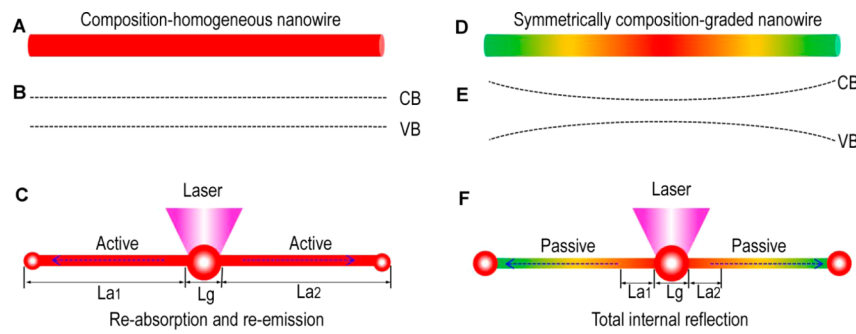


Figure 1. (A) Schematic diagram of a composition-homogeneous NW and (B) its bandgap structure along the axial direction. (C) Schematic waveguiding with local excitation at the center of the NW. The emitted light is actively guided toward the two ends through reabsorption and re-emission. (D) Schematic diagram of a symmetrically composition-graded NW and (E) its graded bandgap structure along the axial direction. (F) Schematic waveguiding with local excitation at the center of the NW. The emitted light is passively guided toward the both ends through total internal reflections. (Lg: Gain length; La1, La2: Absorption length).

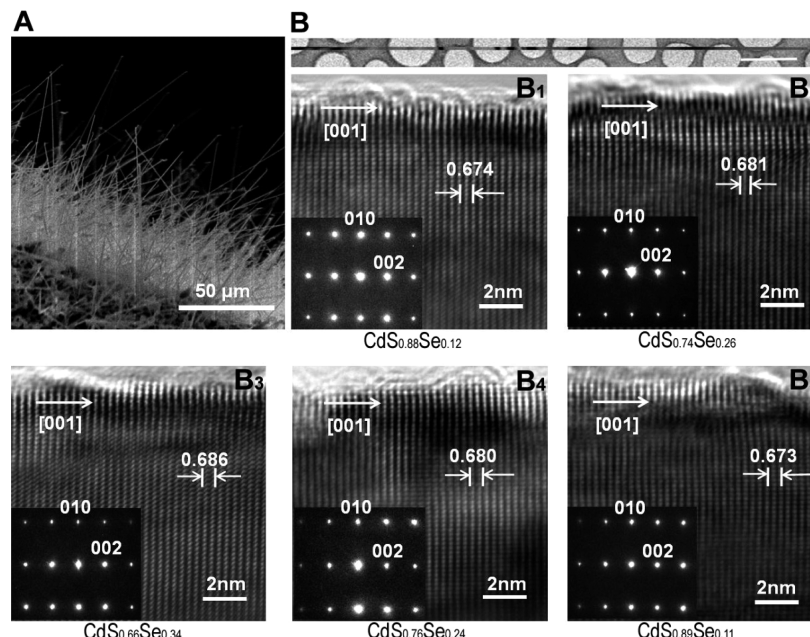


Figure 2. (A) SEM image of the as-grown symmetrically composition-graded NWs. (B) TEM image of a typical symmetrically composition-graded NW (scale bar, 10 μm) and its corresponding HRTEM images and SAED patterns taken from several representative regions along its length. The alloy compositions for each region are shown below the respective images (B₁-B₅).

kind of new nanostructures will help to find more potential applications in constructing novel compact nanophotonic components.

Symmetrical composition-graded CdS_xSe_{1-x} NWs were grown via an evaporation source controlled thermal evaporation route,^{32,33} as schematically shown in Figure S1 (Supporting Information). Briefly, in a horizontal furnace (OTF-1200X) with a 2 in. quartz tube (inner diameter 45 mm, length 150 cm), an alumina boat with CdS powder (Alfa Aesar, 99.999%) was first pulled into the heating zone of the furnace, and the other two boats with CdSe (Alfa Aesar, 99.999%) and CdS powder, respectively, were separated by a quartz rod and placed in the upstream of the tube and located far enough away from the heating zone before growth. A quartz rod driven by step motor through magnetic force was used to push these two boats into/out of the heating zone during the growth. Several silicon wafers coated with 10-nm-thick Au films were placed in the downstream of the gas flow to collect the deposited wires. Before heating, a N₂ flow was introduced into the system at a

rate of 150 sccm for 40 min to eliminate O₂. Then the furnace temperature was ramped to 830 °C at a rate of 40 °C min⁻¹, while maintaining the system pressure at 300 mbar (step 1, Figure S1). After 30 min of growth, pure CdS NWs were obtained and the CdSe boat was smoothly pushed into the heating zone at a rate of 2.3 cm min⁻¹ by the step motor to replace the CdS boat (step 2, Figure S1). After a period time (15–30 min) of growth, unidirectional composition-graded NWs were grown. Meanwhile, the furnace temperature was reduced to 780 °C with a rate of 2 °C min⁻¹. Two minutes later, the other CdS boat was pushed into the heating zone to replace the CdSe boat (step 3, Figure S1) and the growth kept on another period time (15–30 min) while the furnace temperature was slowly increased to 830 °C with a rate of 2 °C min⁻¹. After 30 min of growth at 830 °C (step 3, Figure S1), the furnace was naturally reduced to room temperature.

Scanning electron microscopy (SEM) observation reveals that the as-grown wires have a uniform diameter along their length. The wires have a length of several micrometers and

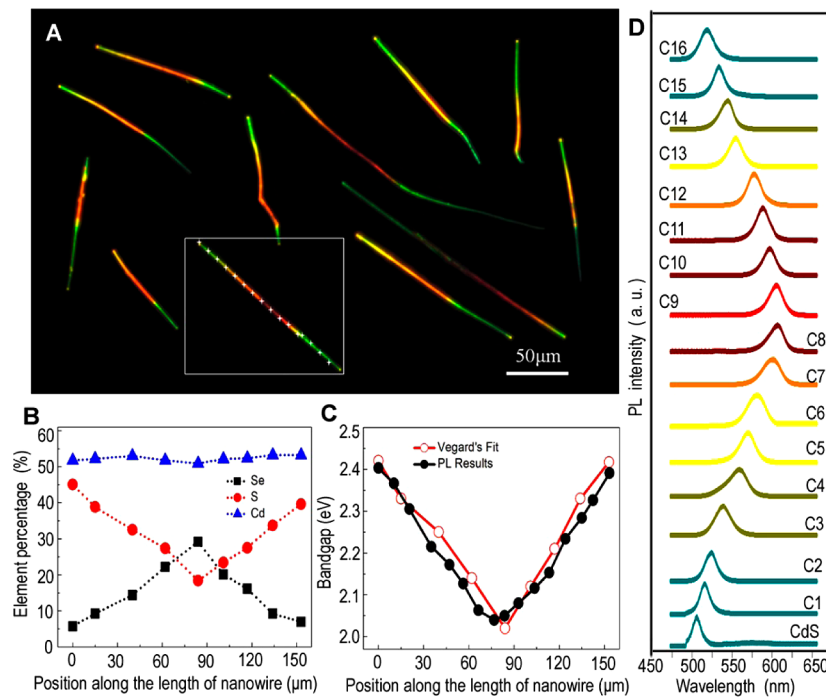


Figure 3. (A) Real-color photograph of some dispersed symmetrically composition-graded NW under illumination of diffused 405 nm laser. These NWs were picked out from the initial grown substrate and dispersed on a transparent MgF_2 wafer. (B) Position-dependent element percentages along the length of the wire for elements Cd, S, and Se, respectively. (C and D) Band gap values and normalized position-dependent PL spectra along the length of a single symmetrically composition-graded NWs which is indicated by a white rectangle box in panel A (see the cross marks for the examined points).

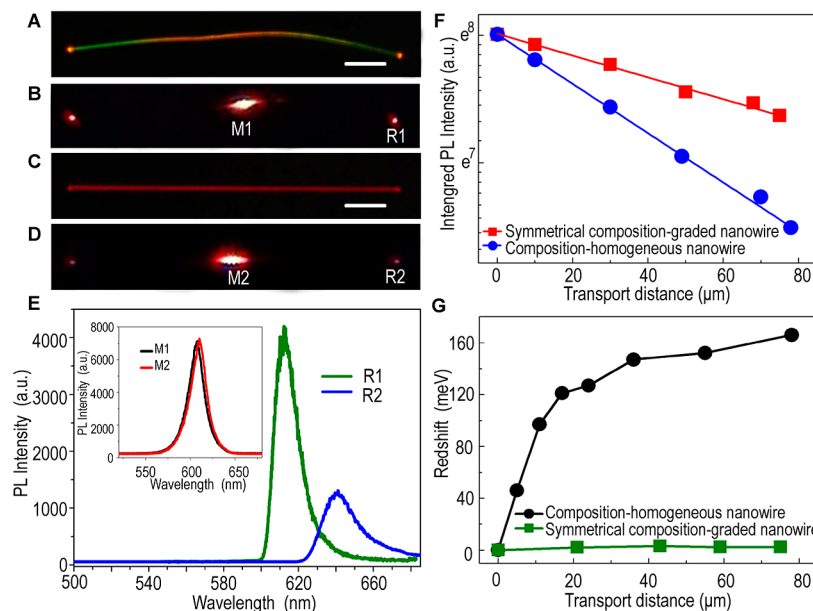


Figure 4. (A, C) Real color photographs of single symmetrically composition-graded NW and composition-homogeneous $\text{CdS}_x\text{Se}_{1-x}$ alloy NW, respectively (scale bar, 20 μm). (B, D) Corresponding PL images when they are locally excited at the central region by the same laser beam (Ar^+ , 488 nm). (E) PL spectra at the excitation position (M1, M2) and output ends (R1, R2) of the NW, respectively (Integration time is 0.5 s in the detection). (F) The propagation distance-dependent intensity of the guided light. (G) Propagation distance-dependent spectral redshift of the detected output signals at the end of the wire. The propagation distance is calculated from the excitation spot (M1 or M2) to the wire end.

diameter ranging from 200 to 1000 nm (Figure 2A), which can be controlled by the size of catalyst and growth time. Figure 2B shows the transmission electron microscopy (TEM) image of a representative NW. The in situ EDS along the total length of a typical wire show that the two ends of the wire contains mainly elements Cd and S, while the central region of the wire is

composed of elements Cd, S, and Se (see the Supporting Information in Figure S2). The S concentration is complementary to that of Se along the length from the central region to the ends, demonstrating that these as-grown wires are symmetrically composition-graded $\text{CdS}_x\text{Se}_{1-x}$ nanostructures. Meanwhile, they are also confirmed by the position-dependent

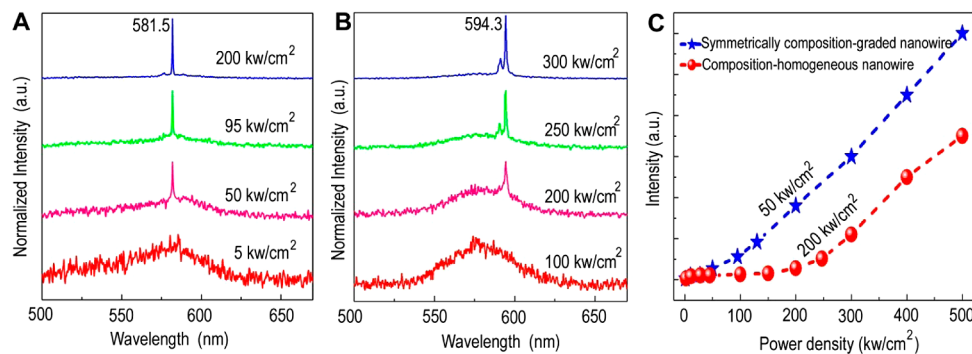


Figure 5. (A and B) Pumping power-dependent PL spectra of single symmetrically composition-graded NW and composition-homogeneous $\text{CdS}_x\text{Se}_{1-x}$ alloy NW at room temperature, respectively (the integration time is 0.01 s in the detection). (C) Pumping power-dependent emission intensity for symmetrically composition-graded NW (blue pentagrams) and composition-homogeneous $\text{CdS}_x\text{Se}_{1-x}$ alloy NW (red spheres), respectively.

element percentages shown in Figure 3B. The corresponding high-resolution TEM (HRTEM) images as well as the selected-area electron diffraction (SAED) patterns (insets) taken from several different locations along the wire are shown in Figure 2B₁–B₅, respectively. The clear lattice profiles are without apparent defects or phase segregations as well as the well-arrayed diffraction spots, indicating that single crystal NWs are high-quality wurtzite structure. The SAED results show that these NWs grow along the [002] direction, and the (002) plane spacing continuously decreases from the central region to the ends along the length. This change in lattice spacing shows good agreement with the gradual transition of S or Se concentration.

Some wires were picked out from the substrate and transferred onto a transparent MgF_2 wafer for optical measurement by using a homemade fiber taper under an optical microscope (Zeiss, Imager A2). The real-color photograph of some selected wires under the illumination of a continuous wave (CW) 405 nm laser was shown in Figure 3A. The emission light of the wire is red at the central region while gradually changed to green at the both ends, which indicating a continuously symmetrical variation of the bandgaps. The spatially resolved microphotoluminescence (μ -PL) spectra collected along the length of a selected wire (see the white cross indicated spots in the rectangle box marked wire in Figure 3A) show that every point of the NW has a single-band PL emission, with peak wavelength gradually changing from ~510 nm at the ends to ~612 nm at the center (Figure 3D). The local bandgap values obtained from the PL spectra have good consistency with those calculated from the EDS results (dots) combined with the Vegard's law for ternary $\text{CdS}_x\text{Se}_{1-x}$ alloys (Figure 3C),^{25,33,34} indicating all of the observed PLs originated from the bandedge transitions of these symmetrically composition-graded alloy NWs. It is noted that the composition along the wire depends on the real deposition temperature along the substrate during the growth, with the x value decreased from the low-temperature region to the high-temperature region. Therefore, the colors (composition) of the examined wires are not all the same, as shown in the real-color photograph (Figure 3A). Especially, the composition at the wire center has some differences for different wires in the examined sample, with the emitting wavelengths ranged from ~580 nm to ~612 nm.

As discussed at the beginning of this paper, the symmetrically composition-graded NWs are expected to be ideal cavities for

low-loss waveguiding. Figure 4A is the real-color PL image of a representative wire, and Figure 4B shows the corresponding PL images when it is locally excited at the central region by the laser beam (Ar^+ , 488 nm). A schematic demonstration of the experimental setup for the optical characterization is shown in Figure S3 (Supporting Information). Figure 4C is the PL image of a composition-homogeneous $\text{CdS}_x\text{Se}_{1-x}$ alloy NW with S mole fraction $x = 0.49$ for comparative study. Figure 4D shows the corresponding PL images when it is locally excited at the central region by the same laser beam as Figure 4B. A portion of the emitted light was guided by the NW cavity and leaked out of the ends. The detected optical intensity at the ends of the symmetrically composition-graded NW is much stronger than that of the composition-homogeneous NW although the emission intensity at the excited locations is kept the same (insert of Figure 4E), indicating the higher waveguiding efficiency of the former. Figure 4E shows the two output PL spectra of the guiding light (R_1 and R_2), which quantitatively confirms that the intensity difference reach ~3.0 folds after transporting ~80 μm . Figure 4F further plots the propagation distance-dependent intensity decay of the guided light. The wires are cut by a homemade wolfram probe during the investigation (see the Supporting Information in Figure S4). The experimental data (dots) can be well fitted into an exponential function, $I = I_0 e^{-\alpha d}$, where I_0 is the initial intensity before guiding, d is the propagation distance from the center of the wire (excitation spot) to the end, and α corresponds to the intensity decay rate. According to this definition, the intensity decay rate of symmetrically composition-graded NW (0.0059, red line) is much smaller than the alloy NW (0.0193, blue line), confirming the waveguiding efficiency can be improved significantly by utilizing a symmetrically composition-graded NW structure. Figure 4G shows the propagation distance-dependent spectral redshift of the guided light along symmetrically composition-graded NW (green line) and the contrasted composition-homogeneous NW (black line), respectively. We can see that the guided light in the symmetrically composition-graded NW almost have no spectrum redshift, while the guided light exhibit a strong redshift during its transportation along the composition-homogeneous NW, due to the reabsorption and re-emitting processes.²⁷ The results further demonstrate that the symmetric wire can efficiently avoid the self-absorption induced energy loss for the excited light at its central region and work as a high efficiency passive waveguide cavity for nanoscale laser.

Figure 5A and B show the pumping power dependent PL spectra for the symmetrically composition-graded NW and composition-homogeneous NW at room temperature, respectively. As can be seen, both wires exhibit broad spontaneous emission bands centered at ~ 580 nm at low pumping power density, and sharp emission lines (581.5 and 594.3 nm, respectively) start to emerge when further increase the pump power to certain levels. Figure 5C shows the intensities of the two sharp emission lines as a function of the pumping power density, both of which exhibit a superlinear increase when the power density above a threshold. The narrow line width and the rapid increase of emission intensity demonstrate that stimulated emission can take place in both wires. However, the laser threshold in symmetrically composition-graded NWs (~ 50 kW cm $^{-2}$) is several times lower than the threshold in composition-homogeneous NWs (~ 200 kW cm $^{-2}$). After examine a dozen of other NWs, the obtained threshold ratio between these two kinds of wires usually has a value ranged from 0.25 to 0.5 depending on the quality of the NW cavity. On the other hand, it is noted that the sharp stimulated emission line always appears at the low energy side of the broad emission band for the homogeneous wires, while at the center for the symmetrical wires, confirming the entirely different optical waveguiding processes.

In general, the round-trip gain should compensate the round-trip loss to achieve laser oscillation in single semiconductor NWs.^{29,35} When laser occurs, the NW can be regarded as two different parts, the gain region and the absorption region, respectively. The condition can be illustrated in the following equation:

$$(e^{g_{th}L_g})^2(e^{-\alpha L_a})^2R^2 = 1$$

where g_{th} is the threshold of the material gain coefficient (the threshold pump intensity is proportional to g_{th}), L_a is the length of absorption region within the NW ($L_a = L_{a1} + L_{a2}$), L_g is the length of gain region, α is the self-absorption coefficient, and R is reflectivity of the two end facets. According to this equation, g_{th} decreases with reducing L_a ; thus the laser threshold decreases with reducing the self-absorption loss.

When the composition-homogeneous CdSSe NW is optically pumped to achieve laser oscillation, the gain region is corresponding to the locally pumped area, which is about 11 μm in the center of the NW (Lg in Figure 1C), and the rest of the wire (La in Figure 1C) all acts as the absorption region during the active process. In comparison, when the symmetrically composition-graded NW is locally pumped at the central region, the gain region is the same as that in the homogeneous NW (Lg in Figure 1F), but the absorption region (La in Figure 1F), however, is much shorter than that in the homogeneous NW. As a result of the continuously increased bandgap value from the center to the two opposite ends, the self-absorption loss of the guided light will reduce to a low level after a much shorter transport distance (La in Figure 1F). On the basis of the above analyses, the greatly shortened absorption region (length) in these symmetrically composition-graded NWs due to the special symmetrical graded-bandgap structure is the key factor that responsible for the lower lasing threshold compared to regular homogeneous NWs. To the best of our knowledge, this is the first work on lowering the NW lasing threshold via reducing the self-absorption loss of the guided light.

In summary, we have designed and realized the growth of symmetrically composition-graded NWs through a multistep moving sources thermal evaporation route. Photoluminescence

measurements show that the emission color of these NWs gradually varied from the red at the central region to the green at the both ends along the length. The symmetrical wire can efficiently avoid the self-absorption induced energy loss for the excited light at its central region and work as a high efficiency passive waveguide cavity. We have further demonstrated that the optically pumping lasing threshold in these symmetrically composition-graded NWs is much lower compared with that of composition-homogeneous NWs. This new nanowire structure shows the potential applications as low-threshold lasers or low-loss waveguides in integrated nanophotonics devices or systems.

■ ASSOCIATED CONTENT

S Supporting Information

Schematic diagram of the experimental setup and growth processes (Figure S1), alloy composition of the NWs (Figure S2), demonstration of the experimental optical characterization (Figure S3), and optical microscopy images of cutting NWs (Figure S4). This material is available free of charge via the Internet at <http://pubs.acs.org>.

■ AUTHOR INFORMATION

Corresponding Author

*E-mail: anlian.pan@hnu.edu.cn.

Author Contributions

P.G., X.Z., and J.X. contributed equally.

Notes

The authors declare no competing financial interest.

■ ACKNOWLEDGMENTS

The authors are grateful to the National Basic Research Program of China (No. 2012CB932703), the NSF of China (Nos. 90923014), the Research Fund for the Doctoral Program of Higher Education (No. 20110161110034), the Aid program for Science and Technology Innovative Research Team in Higher Educational Institutions of Hunan Province, the Scholarship Award for Excellent Doctoral Student granted by Ministry of Education, and the Hunan Provincial Innovation Foundation For Postgraduate (No. CX2012B157) for financial support.

■ REFERENCES

- (1) Xiang, J.; Lu, W.; Hu, Y. J.; Wu, Y.; Yan, H.; Lieber, C. M. *Nature* **2006**, *441*, 489.
- (2) Qian, F.; Li, Y.; Gradečák, S.; Park, H. G.; Dong, Y.; Ding, Y.; Wang, Z. L.; Lieber, C. M. *Nat. Mater.* **2008**, *7*, 701.
- (3) Wu, Y. Y.; Yan, H. Q.; Huang, M.; Messer, B.; Song, J. H.; Yang, P. D. *Chem.—Eur. J.* **2002**, *8*, 1260.
- (4) Jiang, X.; Tian, B.; Xiang, J.; Qian, F.; Zheng, G.; Wang, H.; Mai, L.; Lieber, C. M. *Proc. Natl. Acad. Sci. U.S.A.* **2011**, *108*, 12212.
- (5) Wang, D.; Qian, F.; Yang, C.; Zhong, Z.; Lieber, C. M. *Nano Lett.* **2004**, *4*, 871.
- (6) Service, R. F. *Science* **2010**, *328*, 810.
- (7) Yan, R.; Park, J.-H.; Choi, Y.; Heo, C.-J.; Yang, S.-M.; Lee, L. P.; Yang, P. *Nat. Nanotechnol.* **2012**, *7*, 191.
- (8) Chu, S.; Wang, G.; Zhou, W.; Lin, Y.; Chernyak, L.; Zhao, J.; Kong, J.; Li, L.; Ren, J.; Liu, J. *Nat. Nanotechnol.* **2011**, *6*, 506.
- (9) Sang, H. L.; Takenari, G.; Hiroshi, M.; Jiho, C.; Takafumi, Y. *Nano Lett.* **2010**, *10*, 2038.
- (10) Liu, R. B.; Zhuang, X. J.; Xu, J. Y.; Li, D. B.; Zhang, Q. L.; Ding, K.; He, P. B.; Ning, C. Z.; Zou, B. S.; Pan, A. L. *Appl. Phys. Lett.* **2011**, *99*, 263101.

- (11) Ma, R. M.; Yin, X.; Oulton, R. F.; Sorger, V. J.; Zhang, X. *Nano Lett.* **2012**, *12*, 5396.
- (12) Hua, B.; Motohisa, J.; Kobayashi, Y.; Hara, S.; Fukui, T. *Nano Lett.* **2009**, *9*, 112.
- (13) Xiao, Y.; Meng, C.; Wang, P.; Ye, Y.; Yu, H. K.; Wang, S. S.; Gu, F. X.; Dai, L.; Tong, L. M. *Nano Lett.* **2011**, *11*, 1122.
- (14) Huang, M. H.; Mao, S.; Feick, H.; Yan, H. Q.; Wu, Y. Y.; Kind, H.; Weber, E.; Russo, R.; Yang, P. D. *Science* **2001**, *292*, 1897.
- (15) Johnson, J. C.; Choi, H. J.; Knutson, K. P.; Schaller, R. D.; Yang, P.; Saykally, R. J. *Nat. Mater.* **2002**, *1*, 106.
- (16) Agarwal, R.; Barrelet, C. J.; Lieber, C. M. *Nano Lett.* **2005**, *5*, 917.
- (17) Duan, X. F.; Huang, Y.; Agarwal, R.; Lieber, C. M. *Nature* **2003**, *421*, 241.
- (18) Chu, S.; Wang, G. P.; Zhou, W. H.; Lin, Y. Q.; Chernyak, L.; Zhao, J. Z.; Kong, J. Y.; Li, L.; Ren, J. J.; Liu, J. L. *Nat. Nanotechnol.* **2011**, *6*, 506.
- (19) Zhang, C.; Zou, C. L.; Yan, Y.; Hao, R.; Sun, F. W.; Han, Z. F.; Zhao, Y. S.; Yao, J. *J. Am. Chem. Soc.* **2011**, *133*, 7276.
- (20) Law, M.; Sirbuly, D.; Johnson, J.; Goldberger, J.; Saykally, R.; Yang, P. *Science* **2004**, *305*, 1269.
- (21) Yan, H.; Choe, H. S.; Nam, S. W.; Hu, Y. J.; Das, S.; Klemic, J. F.; Illebogen, J. C.; Lieber, C. M. *Nature* **2011**, *470*, 240.
- (22) Duan, X. F.; Huang, Y.; Cui, Y.; Wang, J. F.; Lieber, C. M. *Nature* **2001**, *409*, 66.
- (23) Friedman, R. S.; McAlpine, M. C.; Ricketts, D. S.; Ham, D.; Lieber, C. M. *Nature* **2005**, *434*, 1085.
- (24) Sirbuly, D. J.; Law, M.; Pauzauskis, P.; Yan, H. Q.; Maslov, A. V.; Knutson, K.; Ning, C. Z.; Saykally, R. J.; Yang, P. D. *Proc. Natl. Acad. Sci. U.S.A.* **2005**, *102*, 7800.
- (25) Pan, A. L.; Zhou, W. C.; Leong, E. S. P.; Liu, R. B.; Chin, A. H.; Zhou, B. S.; Ning, C. Z. *Nano Lett.* **2009**, *9*, 784.
- (26) Pan, A. L.; Liu, R. B.; Zou, B. S. *Appl. Phys. Lett.* **2006**, *88*, 173102.
- (27) Chen, L.; Towe, E. *J. Appl. Phys.* **2006**, *100*, 044305.
- (28) Zou, B. S.; Liu, R. B.; Wang, F.; Pan, A. L.; Cao, L.; Wang, Z. L. *J. Phys. Chem. B* **2006**, *110*, 12865.
- (29) Siegman, A. E. *Lasers*; Oxford University Press: Oxford, 1986.
- (30) Pan, A. L.; Liu, D.; Liu, R. B.; Wang, F. F.; Zhu, X.; Zou, B. S. *Small* **2005**, *1*, 980.
- (31) Pan, A. L.; Wang, X.; He, P. B.; Zhang, Q. L.; Wan, Q.; Zacharias, M.; Zhu, X.; Zou, B. S. *Nano Lett.* **2007**, *7*, 2970.
- (32) Yang, Z. Y.; Xu, J. Y.; Wang, P.; Zhuang, X. J.; Pan, A. L.; Tong, L. M. *Nano Lett.* **2011**, *11*, 5085.
- (33) Gu, F. X.; Yang, Z. Y.; Yu, H.; Xu, J. Y.; Wang, P.; Tong, L. M.; Pan, A. L. *J. Am. Chem. Soc.* **2011**, *133*, 2037.
- (34) Pan, A. L.; Yang, H.; Liu, R. B.; Yu, R.; Zou, B. S.; Wang, Z. L. *J. Am. Chem. Soc.* **2005**, *127*, 15692.
- (35) Zimmler, M. A.; Bao, J.; Capasso, F.; Muller, S.; Ronning, C. *Appl. Phys. Lett.* **2008**, *93*, 051101.